



ORIGINAL ARTICLE

Flower-shaped gold nanoparticles: Preparation, characterization, and electrocatalytic application



Islam M. Al-Akraa ^{a,*}, Ahmad M. Mohammad ^{a,b,*}, Mohamed S. El-Deab ^{a,b},
Bahgat E. El-Anadouli ^b

^a Department of Chemical Engineering, Faculty of Engineering, The British University in Egypt, Cairo 11837, Egypt¹

^b Chemistry Department, Faculty of Science, Cairo University, Cairo 12613, Egypt

Received 19 March 2014; accepted 5 May 2015

Available online 13 May 2015

KEYWORDS

Gold nanoparticles;
Assembling;
Oxygen evolution reaction;
Electrocatalysis

Abstract The modification of a glassy carbon electrode with gold nanoparticles was pursued, characterized, and examined for electrocatalytic applications. The fabrication process of this electrode involved assembling the gold nanoparticles atop of amino group grafted glassy carbon electrode. The scanning electron microscopy indicated the deposition of gold nanoparticles in flower-shaped nanostructures with an average particle size of ca. 150 nm. Interestingly, the electrode exhibited outstanding enhancement in the electrocatalytic activity toward the oxygen evolution reaction, which reflected from the large negative shift (ca. 0.8 V) in its onset potential, in comparison with that observed at the bulk unmodified glassy carbon and gold electrodes. Alternatively, the Tafel plot of the modified electrode revealed a significant increase (~one order of magnitude) in the apparent exchange current density of the oxygen evolution reaction upon the modification, which infers a faster charge transfer. Kinetically, gold nanoparticles are believed to facilitate a favorable adsorption of OH⁻ (fundamental step in oxygen evolution reaction), which allows the charge transfer at reasonably lower anodic polarizations.

© 2015 The Authors. Production and hosting by Elsevier B.V. on behalf of King Saud University. This is an open access article under the CC BY-NC-ND license (<http://creativecommons.org/licenses/by-nc-nd/4.0/>).

1. Introduction

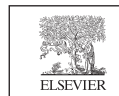
The recent advanced revolution in nanoscience has motivated research in different disciplines from chemistry, physics, materials science, agriculture, medicine, etc. to prepare nanomaterials for prospective applications. In fact, materials in nano-size exhibit unique physical and chemical properties if compared to their bulk entities. Not only geometrically, which is inferred from the unique morphology and the large surface area to volume ratio, but also electronically, the material's properties may change with the shrinkage in particle size (Alivisatos, 1996; Kalimuthu and John, 2008). This has interestingly found

* Corresponding authors at: Suez Desert Road, El Shorouk City, Cairo, Egypt. Tel.: +20 (2) 268 90000x1439; fax: +20 (2) 26875889/97.

E-mail addresses: islam0886@yahoo.com (I.M. Al-Akraa), ammohammad@cu.edu.eg (A.M. Mohammad), msaada68@yahoo.com (M.S. El-Deab), bahgat30@yahoo.com (B.E. El-Anadouli).

¹ www.bue.edu.eg.

Peer review under responsibility of King Saud University.



Production and hosting by Elsevier

potential applications in catalysis (Daniel, 2004; Burda et al., 2005; Kalimuthu and John, 2008), chemical and biochemical sensing (Elghanian et al., 1997; Bharathi et al., 2001; West and Halas, 2003; Aslan et al., 2005; Burda et al., 2005; Stuart et al., 2005; Jena and Raj, 2006; Kalimuthu and John, 2008), and biologic imaging (Bharathi et al., 2001; West and Halas, 2003; Stuart et al., 2005; Jena and Raj, 2006; Maduraiveeran and Ramaraj, 2007; Kalimuthu and John, 2008). In this regard, much of the attention has been dedicated to gold nanoparticles (AuNPs) due to their ease of preparation, high stability and their shape and size-dependent catalytic activity (Sau and Anjali, 2001; Deng et al., 2005; El-Sayed et al., 2005; Jiang et al., 2005; Stuart et al., 2005; Tsunoyama et al., 2005; Hurst et al., 2006; Kalimuthu and John, 2008; Al-Akraa et al., 2011, 2012).

Generally, in order to utilize metal nanoparticles as unique devices, they should be assembled onto electrode surfaces. Several methods are currently available for this purpose, depending on the nature of the electrode material, and the features required. One interesting approach, in this regard, is the electrochemical deposition, which involves the electrochemical reduction of metal ions onto the surface of a conducting material. This procedure has been used to synthesize gold (Finot et al., 1999; El-Deab et al., 2003) and platinum (Manolova et al., 2005) nanoparticles. Another assembling technique involving the “chemical synthesis,” has also been recommended for the synthesis of small-size AuNPs (Frens, 1973; Slot and Geuze, 1985; Brust et al., 1994).

The oxygen evolution reaction (OER) is one of the interesting applications for nanomaterials, where several nano-sized modified electrodes were developed for water electrolyzers (Ma et al., 2006; Guerrini et al., 2007; Singh et al., 2007). The OER represents the principal anodic reaction in water electrolysis, and is a side reaction in a number of anodic processes, e.g., in the chlorine production (Trasatti, 1984). The catalytic activity toward OER has been investigated over a wide range of materials, which are mainly composed of metal, metal oxide, or the alloy of platinum (Birss et al., 1986; Birss and Damjanovic, 1987), gold (Barnartt, 1959), nickel (Bocca et al., 1999; Singh et al., 2007), cobalt (Nidola, 1989; Lee et al., 1996; Wen and Kang, 1998; Bocca et al., 1999), Iridium (Hackwood et al., 1981; Guerrini et al., 2007), ruthenium (Iwakura et al., 1977; Koetz and Stucki, 1985; Birss and Damjanovic, 1987; Ma et al., 2006), and rhodium (O’Sullivan and Burke, 1990). However, unfortunately, the corrosion problems and the parallel oxidation reactions associated with the OER have limited the selection of suitable anodic materials for the development of efficient water electrolyzers. Nano-modified electrodes have then been recommended for OER, and shrinking the particle size of the active electrode was promising to overcome the concerns of efficiency and stability (Sadiek et al., 2012).

In this study, we report on the synthesis, and characterization of flower-shaped AuNPs assembled electrochemically onto glassy carbon (GC) substrate (abbreviated as AuNPs–NH₂/GC). The electrocatalytic activity of this electrode toward OER is investigated in an alkaline medium.

2. Material and methods

Typically-cleaned glassy carbon electrode (GC, $d = 3.0$ mm, purchased from ALS-Japan) with a geometric area of

0.07 cm² was used as the working electrode. A spiral Pt wire and reference hydrogen electrode (RHE) were used as the counter and reference electrodes, respectively.

The assembling of AuNPs atop of the GC electrode was achieved in three consecutive steps (Othman et al., 2009). First, the amino groups were grafted onto the surface of the carbon substrate by holding the GC electrode at $+1.7$ V vs. RHE for 90 min in aqueous solution of ammonium carbamate (99%, Sigma Aldrich) (pH = 8.9) (Uchiyama et al., 2007). Next, a solution of 1.0 mM H₂SO₄ (98%, Fluka) was dropped onto the NH₂-grafted GC electrode (–NH₂/GC) to protonate the –NH₂ group. For anchoring the [AuCl₄][–] ions, the modified GC electrode was then immersed in 1.0 mM H₂SO₄ containing 1.0 mM Na[AuCl₄] (99%, Sigma Aldrich) solution for 10 min followed by washing with 1.0 mM H₂SO₄ to remove the unbounded [AuCl₄][–]. Finally, the anchored [AuCl₄][–] ions were electrochemically reduced in 0.1 mM H₂SO₄ by scanning the potential from ca. 1.1 – 0.4 V vs. RHE at a scan rate of 0.1 V s^{–1} (see the typical cyclic voltammogram (CV) response for this process in Fig. 2). A single rather broad reduction peak is observed at ca. 0.84 V during the first CV cycle with a charge of 74.6 μC. This peak is assigned to the reduction of the anchored [AuCl₄][–] to Au⁰. The absence of this reduction peak during the second CV cycle suggested the exclusive reduction of all the complexed [AuCl₄][–] during the first cycle.

For the sake of comparison, a bulk-Au electrode ($d = 1.6$ mm in diameter-purchased from ALS-Japan) was polished with a fine emery paper and subsequently with aqueous slurries of successively fine alumina powder with the help of a polishing microcloth. Then, the electrode was washed with doubly distilled water to remove the adsorbed alumina particles. The bulk Au electrode was next cleaned electrochemically in 0.5 M H₂SO₄ by cycling the potential sweep between 0 and 1.7 V vs. RHE at a scan rate of 1 V s^{–1} for 10 min or until the characteristic CV of a clean Au was obtained.

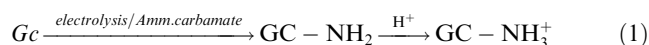
The electrochemical measurements were performed at room temperature (25 ± 1 °C) in a conventional two-compartment three electrode glass cell using an EG&G potentiostat (model 273A) operated with Echem 270 software. A field emission scanning electron microscope (FE-SEM, QUANTA FEG 250) was employed to evaluate the electrode’s morphology. All of the chemicals used in this investigation were of high purity and used without further purification.

3. Results and discussion

3.1. Preparation and characterization of AuNPs–NH₂/GC electrode

The three-steps procedure employed for fabricating AuNPs atop of the NH₂-grafted GC electrode can be described as follows (Othman et al., 2009):

- (1) –NH₂ grafting and protonation:



Herein, the amino groups were grafted onto the surface of the carbon substrate (details are provided in the experimental section). The current transient is shown in Fig. 1, from which the total charge ($Q_{total} = Q_{oxidation} + Q_{charging} + Q_{NH_2}$) of

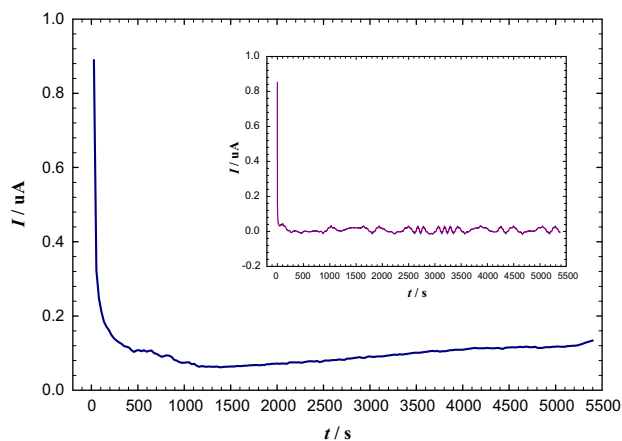


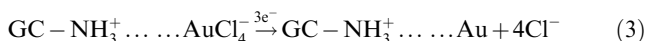
Figure 1 Current transient for the $-\text{NH}_2$ group grafting of the GC electrode in 0.1 M ammonium carbamate solution (pH = 8.9) at a constant potential of +1.7 V vs. RHE. The inset represents the current transient curve in aqueous solution of 0.1 M Na_2SO_4 (pH = 8.9) at a constant potential of +1.7 V vs. RHE.

503 μC is estimated. It is valuable here to refer that this charge is distributed, albeit, unequally between the surface oxidation and charging of GC electrode and the insertion of $-\text{NH}_2$ groups. Recording the current transient for a blank solution of 0.1 M Na_2SO_4 at the same pH of 8.9 assisted in the estimation of Q_{blank} ($Q_{\text{oxidation}} + Q_{\text{charging}}$) which valued 177 μC , as estimated from the inset of Fig. 1. Thus, Q_{NH_2} can be evaluated by ($Q_{\text{total}} - Q_{\text{blank}} = 326 \mu\text{C}$).

(2) Electrostatic binding:



(3) Electrochemical reduction:



The anchored $[\text{AuCl}_4]^-$ ions were electrochemically reduced (see details in the experimental section). The typical cyclic voltammogram (CV) response for this process is depicted in

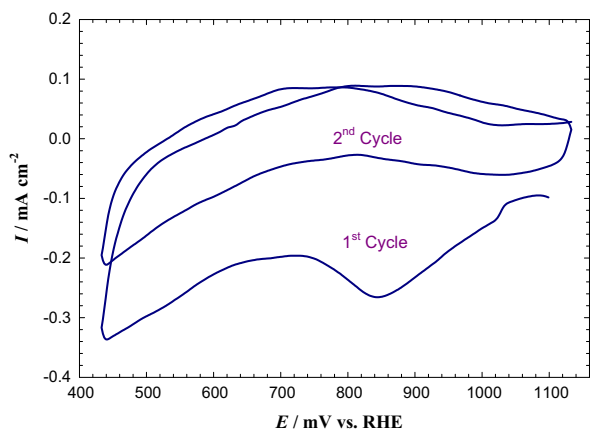


Figure 2 CV response obtained at $-\text{NH}_2/\text{GC}$ electrode in 0.1 mM H_2SO_4 after complexation in 1 mM $\text{H}_2\text{SO}_4 + 1 \text{ mM Na}[\text{AuCl}_4]$ for 10 min. Potential scan rate is 100 mV s^{-1} .

Fig. 2. A single rather broad reduction peak is observed at ca. 0.84 V during the first CV cycle with a charge of 74.6 μC . This peak is assigned to the reduction of the anchored $[\text{AuCl}_4]^-$ to Au^0 . The absence of this reduction peak during the second CV cycle suggested the exclusive reduction of all the complexed $[\text{AuCl}_4]^-$ during the first cycle.

The SEM image captured for $\text{AuNPs}-\text{NH}_2/\text{GC}$ electrode confirmed the deposition of homogeneous and well-separated (no aggregation) AuNPs in flower-shaped geometry with an average particle size of ca. 150 nm (compare Fig. 3c for $\text{AuNPs}-\text{NH}_2/\text{GC}$ electrode with those for bare GC (Fig. 3a) and $-\text{NH}_2/\text{GC}$ (Fig. 3b) electrodes).

Alternatively, a comparison of the CVs of the modified and unmodified GC electrodes has further confirmed the successful deposition of AuNPs onto the GC surface. Fig. 4 shows the characteristic CV obtained at the bare GC and $\text{AuNPs}-\text{NH}_2/\text{GC}$ in Ar-saturated 0.5 M H_2SO_4 . The characteristic peaks of Au were totally absent in the CV response at the bare GC electrode (Fig. 4a), whereas, after assembling the AuNPs, the typical characteristic CV of Au substrate (Fig. 4b) appeared, with the surface oxidation starting from $\sim 1.3 \text{ V}$ and the oxide reduction at $\sim 1.1 \text{ V}$. These peaks appeared almost at the same potentials of a clean bulk Au electrode (see inset of Fig. 4) (Al-Akraa et al., 2013), but the peak currents depended on the surface area. One can clearly notice the intensive enhancement in OER in the anodic potential sweep after 1.4 V at $\text{AuNPs}-\text{NH}_2/\text{GC}$ (Fig. 4b), in comparison with that at the bare Au electrode (inset of Fig. 4). The real surface area of the AuNPs was 0.03 cm^2 , as estimated from the charge consumed during the reduction of the Au surface oxide (see Fig. 4b) using $400 \mu\text{C cm}^{-2}$ as a reported value (Trasatti and Petrii, 1991).

Moreover, the CV measurements of $[\text{Fe}(\text{CN})_6]^{3-/4-}$ couple were performed to track the reversibility of the $\text{Fe}^{3+}/\text{Fe}^{2+}$ redox reaction over the unmodified and the modified electrodes. Fig. 5 shows the CVs at a scan rate of 150 mV s^{-1} in 1 mM $\text{K}_3[\text{Fe}(\text{CN})_6]$ in 0.1 M KCl at the bare GC, $-\text{NH}_2/\text{GC}$, and $\text{AuNPs}-\text{NH}_2/\text{GC}$ electrodes. A typical well-defined reversible voltammogram characteristic of a diffusion-controlled redox process was observed at the bare GC electrode with a ΔE_p value of ca. 70 mV vs. RHE (Fig. 5a). Whereas after grafting of the NH_2 group atop of the GC electrode (Fig. 5b), the redox peaks of $[\text{Fe}(\text{CN})_6]^{3-/4-}$ became ill-defined with a ΔE_p value of ca. 130 mV vs. RHE and the charging current increased compared to the bare GC electrode, which may be attributed to the existence of the $-\text{NH}_2$ hydrophilic groups as well as the oxidation of the GC surface. After immobilization of AuNPs (Fig. 5c), the redox peaks returned back to its original case observed at the bare GC but with a higher charging current, which confirms the successful immobilization of AuNPs atop of the $-\text{NH}_2/\text{GC}$ electrode.

3.2. Electrocatalytic activity toward the OER

The OER is an anodic process, which takes place at most of the metal electrode surfaces at potentials sufficiently anodic to permit the formation of various kinds of oxides. The electrocatalytic activity of the $\text{AuNPs}-\text{NH}_2/\text{GC}$ electrode toward the OER was examined in Ar-saturated 0.5 M KOH solution. Fig. 6 shows the linear sweep voltammograms (LSVs) at a

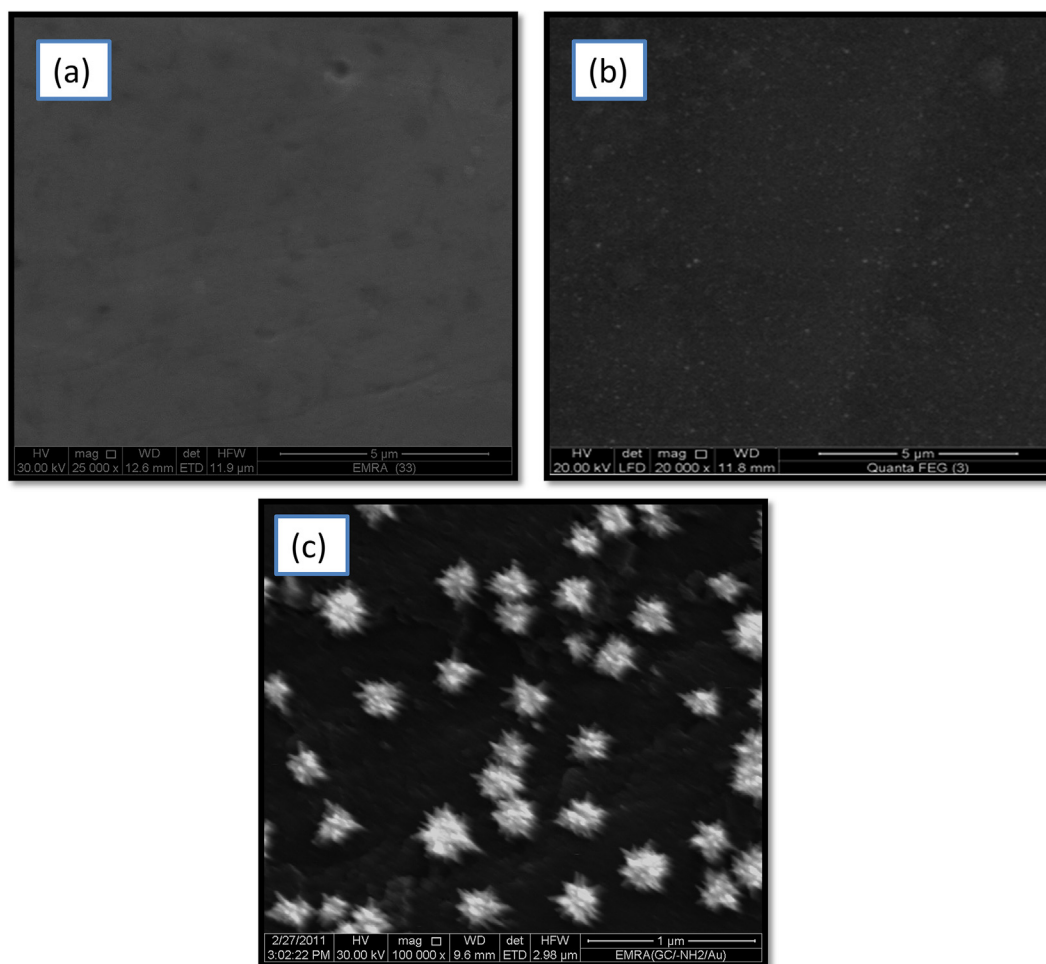


Figure 3 FE-SEM micrographs of (a) bare GC, (b) $-\text{NH}_2/\text{GC}$, and (c) $\text{AuNPs}-\text{NH}_2/\text{GC}$ electrodes.

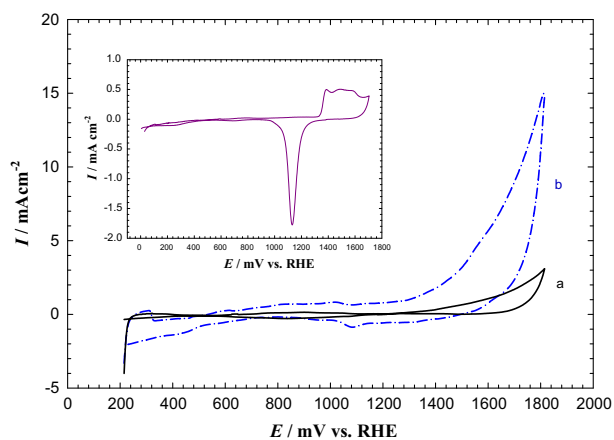


Figure 4 CV measured in Ar-saturated $0.5 \text{ M H}_2\text{SO}_4$ at 100 mV s^{-1} for (a) bare GC and (b) $\text{AuNPs}-\text{NH}_2/\text{GC}$ electrodes (grafting has been achieved in carbamate solution for 90 min). The inset is the CV measured in Ar-saturated $0.5 \text{ M H}_2\text{SO}_4$ at 100 mV s^{-1} for bulk Au electrode ($d = 1.6 \text{ mm}$).

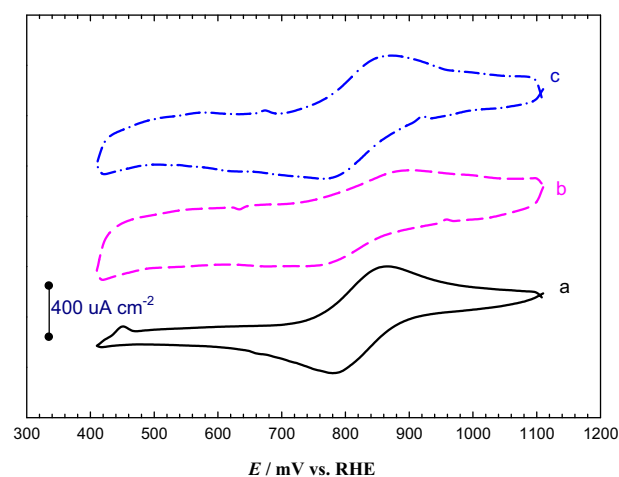


Figure 5 CV obtained in $1 \text{ mM K}_3[\text{Fe}(\text{CN})_6]$ in 0.1 M KCl solution for (a) bare GC, (b) $-\text{NH}_2/\text{GC}$, and (c) $\text{AuNPs}-\text{NH}_2/\text{GC}$ electrodes. Potential scan rate is 150 mV s^{-1} .

potential scan rate of 0.02 V s^{-1} for the OER at bare GC, bulk Au, and AuNPs-NH₂/GC electrodes. In fact, the linear sweep voltammetry is one of the interesting electrochemical approaches that can easily compare between the electrocatalytic activities of different electrode materials toward certain electrochemical reactions.

For anodic reactions, as in case of the OER, the lower the onset potential (the potential at which the reaction starts) for a given reaction the electrode has, the better the electrocatalytic enhancement the electrode exhibits. This is simply because the negative shift in the onset potential will directly be reflected in a power saving which is ultimately targeted for industrial applications. The OER started at ca. 2.5 V vs. RHE at the bare GC electrode (Fig. 6a). However, it started at a lower value of ca. 2.2 V vs. RHE, at the bulk Au electrode (Fig. 6b) (Mohammad et al., 2008). Interestingly, after assembling the AuNPs, the AuNPs-NH₂/GC electrode exhibited a significant enhancement in the electrocatalytic activity toward OER (Fig. 6c). It can be seen that the onset potential for the OER at AuNPs-NH₂/GC electrode is negatively shifted by ca. 0.8 V and ca. 0.5 V if compared, respectively, to the bare GC and bulk Au electrodes. It is anticipated that this noteworthy negative shifts in the onset potential of the current flow for the OER on the AuNPs-NH₂/GC electrode will lead to a significant power saving for commercial electrolyzers.

The stability of the modified electrodes has been examined by recording the current transients (*i-t*) for the OER in Ar-saturated 0.5 M KOH solution at bare GC, bulk Au, and AuNPs-NH₂/GC electrodes at an anodic potential of 1.9 V. Fig. 7 shows that bare GC and bulk Au electrodes did not show any activity at the applied potential (Fig. 7a and b). This matches with the recorded data of Fig. 6a and b. Interestingly, AuNPs-NH₂/GC electrode showed a higher activity compared with that of bare GC and bulk Au electrodes (compare Fig. 7c with a and b) but, unfortunately, this activity decreased gradually with time due to the accumulation of the generated oxygen gas bubbles at the electrode surface. This can lead to either decreasing the effective surface area of the modified electrode or reducing the mechanical stability of the AuNPs and thus lowers the overall catalytic performance of the modified electrode (Mohammad et al., 2008).

3.3. Origin of the electrocatalytic enhancement of the OER

The unique electrocatalytic activity observed on the AuNPs-NH₂/GC electrode for the OER can be explained considering the general mechanism for the OER that has been frequently considered in alkaline media (Matsumoto et al., 1980; Rasiyah et al., 1982; Ferreria et al., 1988):



Here M refers to metal active surface site. The rate determining step for the OER is frequently assigned to the adsorption and the initial charge transfer, i.e., Reaction (4) (Mohammad et al., 2008). Similar moderate catalytic response (ca. 0.3 V compared to the onset potential obtained on the

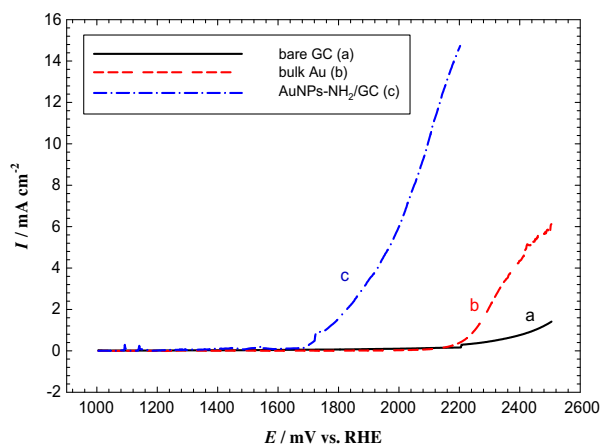


Figure 6 LSVs obtained for the OER in Ar-saturated 0.5 M KOH solution at (a) bare GC, (b) bulk Au, and (c) AuNPs-NH₂/GC electrodes. Potential scan rate is 20 mV s^{-1} .

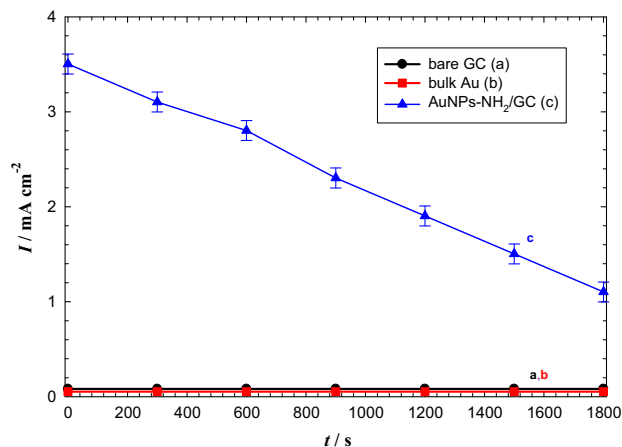


Figure 7 Current transients (*i-t*) measured at 1.9 V for the OER in Ar-saturated 0.5 M KOH solution at (a) bare GC, (b) bulk Au, and (c) AuNPs-NH₂/GC electrodes.

bare GC) was also observed at the manganese oxide NPs-modified GC electrode, and the charge transfer step (Reaction (4)) was similarly assigned as the rate determining step (Rueutschi and Delahay, 1955; Mohammad et al., 2008). Therein, the catalytic enhancement was believed to originate from a redox mediation by the manganese oxide (Mohammad et al., 2008). In the current case, it is expected that the surface structure is changed upon assembling the AuNPs to provide more adsorption sites for the adsorption of OH⁻. This can, definitely, facilitate the charge transfer at the rate determining step (Reaction (4)), and will certainly enhance the OER.

Alternatively, the Tafel plots were measured to account on the charge transfer and mechanism of OER. Interestingly, the Tafel plots for the bulk Au and AuNPs-NH₂/GC electrodes were parallel to each other with a slope close to 120 mV/decade (see Fig. 8), and both were consistent with the reported study claiming that Reaction (4) is the rate determining step for OER in alkaline media (Mohammad et al., 2008; Sadiek et al., 2012). Furthermore, the apparent exchange

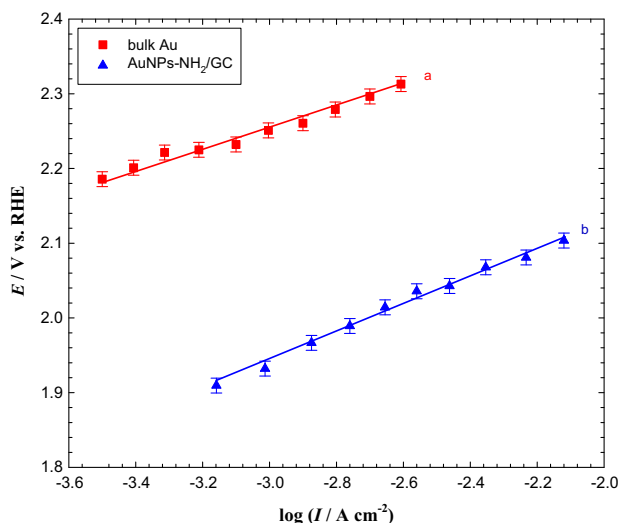


Figure 8 Tafel plots for the OER in Ar-saturated 0.5 M KOH solution at (a) bulk Au and (b) AuNPs–NH₂/GC electrodes.

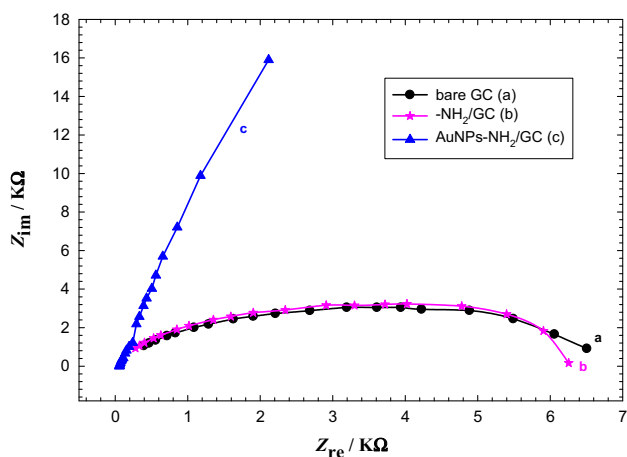


Figure 9 Nyquist plots obtained in Ar-saturated 0.5 M KOH solution recorded at AC potential amplitude of 1.8 V for (a) bare GC, (b) –NH₂/GC, and (c) AuNPs–NH₂/GC electrodes. Frequency range from 10 mHz to 100 kHz.

current density of the OER at the AuNPs–NH₂/GC electrode was higher approximately by one order of magnitude than that estimated at the bulk Au electrode (see Fig. 8). This again supports the faster and favorable charge transfer at the AuNPs-modified electrode.

Electrochemical impedance spectroscopy (EIS) is a very useful tool for the investigation of the electrochemical behavior of electrode surface (Yavuz et al., 2015). Fig. 9 shows the EIS results of bare GC, –NH₂/GC, and AuNPs–NH₂/GC electrodes in Ar-saturated 0.5 M KOH solution recorded at AC potential amplitude of 1.8 V at a frequency range from 10 mHz to 100 kHz. The charge transfer resistance (R_{ct}) which controls the charge transfer kinetics at the electrode surface is equal to the semicircle diameter of the Nyquist plots (Yang et al., 2013). It is clear that the value of the R_{ct} at the AuNPs–NH₂/GC electrode, where Nyquist diagram is almost straight line, is much less than that obtained at bare GC,

–NH₂/GC electrodes implying a facilitated charge transfer rate and thus improving, effectively, the conductivity of the modified AuNPs–NH₂/GC electrode (Yang et al., 2013; Yavuz et al., 2015).

3.4. Energy saving

The significant decrease in the anodic potential obtained after the modification with AuNPs corresponds to a reduction in the energy consumption at the anode and consequently, decreases the overall energy consumption in the electrolysis process. The energy saving in watt hours, $\Delta W_{(a)}$, at the anode at a particular current, i , is given by:

$$\Delta W_{(a)} = \frac{i\Delta E_{(a)}t}{3600} \quad (8)$$

where t is the electrolysis time in seconds, $\Delta E_{(a)}$ is the shift in the potential at a particular current at the anode upon the modification with AuNPs. The values of $\Delta E_{(a)}$ were obtained as described in Section 3.2. The amount of oxygen gas produced (g equiv.) is given by Faraday's law as (it/F) . Consequently, the energy saving at a current density of 5 mA cm^{-2} , P , at the anode in kW h per Kilogram of oxygen gas is given by:

$$P = \frac{i\Delta E_{(a)}(t/3600)}{i(t/F)} = \frac{\Delta E_{(a)}F}{3600} \quad (9)$$

It is valuable here to say that energy with values 21.4 and 13.4 kW h/kg of O₂ gas is saved when comparing AuNPs–NH₂/GC electrode with bare GC and bulk Au electrodes respectively. This highlights the excellent performance of the modified AuNPs–NH₂/GC electrode toward the OER.

4. Conclusions

Flower-shaped AuNPs with an average particle size of ca. 150 nm have been synthesized atop of amino group-grafted GC electrode. A significant enhancement in the electrocatalytic activity of this modified AuNPs–NH₂/GC electrode toward OER has been observed with a negative shift of $\sim 0.8 \text{ V}$ and $\sim 0.5 \text{ V}$ in the onset potential, respectively in comparison with the bare GC and bulk Au electrodes. This can, consequently, provide an energy saving of 21.4 and 13.4 kW h/kg of O₂ gas at a current density of 5 mA cm^{-2} on the AuNPs–NH₂/GC electrode, respectively, if compared to bare GC and bulk Au electrodes. The AuNPs are proposed to facilitate the favorable adsorption of OH[–]. Thus, the charge transfer during the conversion of water into molecular oxygen can be achieved at reasonably lower anodic polarizations.

References

- Al-Akraa, I.M., Mohammad, A.M., El-Deab, M.S., El-Anadouli, B.E., 2011. Electrooxidation of formic acid at platinum–gold nanoparticle-modified electrodes. *Chem. Lett.* 40, 1374–1375.
- Al-Akraa, I.M., Mohammad, A.M., El-Deab, M.S., El-Anadouli, B.E., 2012. Development of tailor-designed gold–platinum nanoparticles binary catalysts for efficient formic acid electrooxidation. *Int. J. Electrochem. Sci.* 7, 3939–3946.
- Al-Akraa, I.M., Mohammad, A.M., El-Deab, M.S., El-Anadouli, B.E., 2013. Self-assembling of gold nanoparticles array for electro-sensing applications. *Int. J. Electrochem. Sci.* 8, 458–466.

- Alivisatos, A., 1996. Semiconductor clusters, nanocrystals, and quantum dots. *Science* 271, 933–937.
- Aslan, K., Lakowicz, J., Geddes, C., 2005. Nanogold plasmon resonance-based glucose sensing. 2. Wavelength-ratiometric resonance light scattering. *Anal. Chem.* 77, 2007–2014.
- Barnartt, S., 1959. The oxygen-evolution reaction at gold anodes: I. Accuracy of overpotential measurements. *J. Electrochem. Soc.* 106, 722–729.
- Bharathi, S., Nagami, M., Lev, O., 2001. Electrochemical organization of gold nanoclusters in three dimensions as thin films from an aminosilicate-stabilized gold sol and their characterization. *Langmuir* 17, 2602–2609.
- Birss, V.I., Damjanovic, A., 1987. Oxygen evolution at platinum electrodes in alkaline solutions: I. Dependence on solution pH and oxide film thickness. *J. Electrochem. Soc.* 134, 113–117.
- Birss, V.I., Damjanovic, A., Hudson, P.G., 1986. Oxygen evolution at platinum electrodes in alkaline solutions: II. Mechanism of the reaction. *J. Electrochem. Soc.* 133, 1621–1625.
- Bocca, C., Barbucci, A., Delucchi, M., Cerisola, G., 1999. NICKEL-COBALT oxide-coated electrodes: influence of the preparation technique on oxygen evolution reaction (OER) in an alkaline solution. *Int. J. Hydrogen Energy* 24, 21–26.
- Brust, M., Walker, M., Bethell, D., Schiffrin, D., Whyman, R., 1994. Synthesis of thiol-derivatized gold nanoparticles in a two phase liquid-liquid system. *J. Chem. Soc.*, 801–802
- Burda, C., Chen, X., Narayanan, R., El-Sayed, M., 2005. Chemistry and properties of nanocrystals of different shapes. *Chem. Rev.* 105, 1025–1102.
- Daniel, M.C.A.D., 2004. Gold nanoparticles: assembly, supramolecular chemistry, quantum-size related properties and applications toward biology, catalysis and nanotechnology. *Chem. Rev.* 104, 293–346.
- Deng, J.-P., Shih, W.-C., Mou, C.-Y., 2005. Hydrogenation of Anthracene catalyzed by surfactant-protected gold nanoparticles in aqueous solution: size dependence. *Chem. Phys. Chem.* 6, 2021–2025.
- El-Deab, M.S., Okajima, T., Ohsaka, T., 2003. Electrochemical reduction of oxygen on gold nanoparticles-electrodeposited glassy carbon electrodes. *J. Electrochem. Soc.* 150, A851–857.
- Elghanian, R., Storhoff, J., Mucic, R., Letsinger, R., Mirkin, C., 1997. Selective colorimetric detection of polynucleotides based on the distance-dependent optical properties of gold nanoparticles. *Science* 277, 1078–1081.
- El-Sayed, I., Huange, X., El-Sayed, M., 2005. Surface plasmon resonance scattering and absorption of anti-EGFR antibody conjugated gold nanoparticles in cancer diagnostics: applications in oral cancer. *Nano Lett.* 5, 829–834.
- Ferreria, A.C., Gonzalez, E.R., ticianelli, E.A., Avaca, L.A., Matvienko, B., 1988. The effect of temperature on the water electrolysis reactions on nickel and nickel-based codeposits. *J. Appl. Electrochem.* 18, 894–898.
- Finot, M.O., Braybrook, G.D., McDermott, M.T., 1999. Characterization of electrochemically deposited gold nanocrystals on glassy carbon electrodes. *J. Electroanal. Chem.* 466, 234–241.
- Frens, G., 1973. Controlled nucleation for the regulation of the particle size in monodisperse gold suspensions. *Nature* 241, 20–22.
- Guerrini, E., Chen, H., Trasatti, S., 2007. Oxygen evolution on aged IrOx/Ti electrodes in alkaline solutions. *J. Solid State Electrochem.* 11, 939–945.
- Hackwood, S., Schiavone, L.M., Dautremont-Smith, W.C., Beni, G., 1981. Anodic evolution of oxygen on sputtered iridium oxide films. *J. Electrochem. Soc.* 128, 2569–2573.
- Hurst, S., Lytton-Jean, A., Mirkin, C., 2006. Maximizing DNA loading on a range of gold nanoparticle sizes. *Anal. Chem.* 78, 8313–8318.
- Iwakura, C., Hirao, K., Tamura, H., 1977. Anodic evolution of oxygen on ruthenium in acidic solutions. *Electrochim. Acta* 22, 329–334.
- Jena, B., Raj, C., 2006. Electrochemical biosensor based on integrated assembly of dehydrogenase enzymes and gold nanoparticles. *Anal. Chem.* 78, 6332–6339.
- Jiang, X., Jiang, J., Jin, Y., Wang, E., Dong, S., 2005. Effect of colloidal gold size on the conformational changes of adsorbed cytochrome c: probing by circular dichroism, UV-visible, and infrared spectroscopy. *Biomacromolecules* 6, 46–53.
- Kalimuthu, P., John, S., 2008. Size dependent electrocatalytic activity of gold nanoparticles immobilized onto three dimensional sol-gel network. *J. Electroanal. Chem.* 617, 164–170.
- Koetz, R., Stucki, S., 1985. Oxygen evolution and corrosion on ruthenium-iridium alloys. *J. Electrochem. Soc.* 132, 103–107.
- Lee, Y.-S., Hu, C.-C., Wen, T.-C., 1996. Oxygen evolution on Co-Cu-Zn ternary spinel oxide-coated electrodes in alkaline solution: integration of statistical, electrochemical, and textural approaches. *J. Electrochem. Soc.* 143, 1218–1225.
- Ma, H., Liu, C., Liao, J., Su, Y., Xue, X., Xing, W., 2006. Study of ruthenium oxide catalyst for electrocatalytic performance in oxygen evolution. *J. Mol. Catal. A: Chem.* 247, 7–13.
- Maduraiveeran, G., Ramaraj, R., 2007. Gold nanoparticles embedded in silica sol-gel matrix as an amperometric sensor for hydrogen peroxide. *J. Electroanal. Chem.* 608, 52–58.
- Manolova, M., Ivanova, V., Kolb, D.M., Boyen, H.G., Ziemann, P., Buttner, M., Romayuk, A., Oelhafen, P., 2005. Metal deposition onto thiol-covered gold: platinum on a 4-mercaptopyridine SAM. *Surf. Sci.* 590, 146–153.
- Matsumoto, Y., Yamada, S., Nishida, T., Sato, E., 1980. Oxygen evolution on La_{1-x}Sr_xFe_{1-y}Co_yO₃ series oxides. *J. Electrochem. Soc.* 127, 2360–2364.
- Mohammad, A.M., Awad, M.I., El-Deab, M.S., Okajima, T., Ohsaka, T., 2008. Electrocatalysis by nanoparticles: optimization of the loading level and operating pH for the oxygen evolution at crystallographically oriented manganese oxide nanorods modified electrodes. *Electrochim. Acta* 53, 4351–4358.
- Nidola, A., 1989. Electrode materials for oxygen evolution cobalt treated lead vs. commercial lead and lead alloys. *Mater. Chem. Phys.* 22, 183–201.
- O'Sullivan, E.J.M., Burke, L.D., 1990. Kinetics of oxygen gas evolution on hydrous rhodium oxide films. *J. Electrochem. Soc.* 137, 466–471.
- Othman, S.H., El-Deab, M.S., Okajima, T., Ohsaka, T., 2009. Novel procedure for the fabrication of gold nanostructures enriched in Au (110) facet orientation. *Electrochem. Commun.* 11, 1273–1276.
- Rasyiah, P., tseung, A.C.C., Hibbert, D.B., 1982. A mechanistic study of oxygen evolution on NiCo₂O₄: I. Formation of higher oxides. *J. Electrochem. Soc.* 129, 1724–1727.
- Rueutschi, P., Delahay, P., 1955. Influence of electrode material on oxygen overvoltage: a theoretical analysis. *J. Chem. Phys.* 23, 556–560.
- Sadieq, I.M., Mohammad, A.M., El-Shakre, M.E., El-Deab, M.S., 2012. Electrocatalytic activity of nickel oxide nanoparticles-modified electrodes: optimization of the loading level and operating pH towards the oxygen evolution reaction. *Int. J. Hydrogen Energy* 37, 68–77.
- Sau, T.K., Anjali, T.P., 2001. Size regime dependent catalysis by gold nanoparticles for the reduction of eosin. *J. Phys. Chem. B* 105, 9266–9272.
- Singh, R.N., Sharma, T., Singh, A., 2007. Electrocatalytic properties of perovskite type La_{2-x}Sr_xNiO₄ (0 ≤ x ≤ 1.0) obtained by the citric acid sol-gel precursor route for oxygen evolution in KOH solutions. *New Mater. Electrochem. Syst.* 10, 105–111.
- Slot, J.W., Geuze, H.J., 1985. A new method for preparing gold probes for multiple-labeling cytochemistry. *Eur. J. Cell Biol.* 38, 87–93.
- Stuart, D., Haes, A., Yonzon, C., Hicks, E., Duyne, R., 2005. Biological applications of localised surface plasmonic phenomena. *IEEE Proc. Nanobiotechnol.* 152, 13–32.
- Trasatti, S., 1984. Electrocatalysis in the anodic evolution of oxygen and chlorine. *Electrochim. Acta* 29, 1503–1512.

- Trasatti, S., Petrii, O.A., 1991. Real surface area measurements in electrochemistry. *Pure Appl. Chem.* 63, 711–734.
- Tsunoyama, H., Sakurai, H., Negishi, Y., Tsukuda, T., 2005. Size-specific catalytic activity of polymer-stabilized gold nanoclusters for aerobic alcohol oxidation in water. *J. Am. Chem. Soc.* 127, 9374–9375.
- Uchiyama, S., Watanabe, H., Yamazaki, H., Kanazawa, A., Hamana, H., Okabe, Y., 2007. Electrochemical introduction of amino group to a glassy carbon surface by the electrolysis of carbamic acid. *J. Electrochem. Soc.* 154, F31–F35.
- Wen, T.-C., Kang, H.-M., 1998. Co–Ni–Cu ternary spinel oxide-coated electrodes for oxygen evolution in alkaline solution. *Electrochim. Acta* 43, 1729–1745.
- West, J., Halas, N., 2003. Engineered nanomaterials for biophotonics applications: improving sensing, imaging, and therapeutics. *Annu. Rev. Biomed. Eng.* 5, 285–292.
- Yang, C., Chai, Y., Yuan, R., Xu, W., Chen, S., 2013. Gold nanoparticles-graphene nanohybrid bridged 3-amino-5-mercapto-1,2,4-triazole-functionalized multiwall carbon nanotubes for the simultaneous determination of hydroquinone, catechol, resorcinol and nitrite. *Anal. Methods* 5, 666–672.
- Yavuz, E., Ozdokur, K., Cakar, I., Kocak, S., Ertas, F., 2015. Electrochemical preparation, characterization of molybdenum-oxide/platinum binary catalysts and its application to oxygen reduction reaction in weakly acidic medium. *Electrochim. Acta* 151, 72–80.